Papers submitted to the Conference "Applications of Physics in Mechanical and Material Engineering"

Modeling of the Rolling Friction Torque in Contact Zone of a Cylinder–Flat Surface for Meso-Structural Bodies

S. Śpiewak*

Czestochowa University of Technology, Faculty of Mechanical Engineering and Computer Science, Dąbrowskiego 73, 42-201 Częstochowa, Poland

Doi: 10.12693/APhysPolA.142.63 *e-mail: szczepan.spiewak@pcz.pl

The way of modeling the contact phenomena of two bodies — with a finite and infinite radius of curvature — is presented in the paper. The basic method used in the research was the finite element method. A model to simulate deformations occurring during rotational and translational movement of a wheel on a flat surface was developed. The research was based on the own design solution of the mobile platform's running gear. The model takes into account all geometrical parameters, the flexibility of the contact zone loaded, and orthotropic material properties of the analyzed meso-structural bodies. The work contains the values of all parameters of the material model that were obtained experimentally. The final result of the study was to determine the relationship between rolling resistance and external loads.

topics: friction torque, finite element method, meso-structure, acrylonitrile butadiene styrene

1. Introduction

The development of electromobility is related to the technique of controlling the movement of vehicles. One of the elements of effective control is the examination of the physical phenomenon associated with the movement. Moreover, identifying the constants and variables parameters is necessary to describe the state of the object. For this purpose, there is a need to develop models which can map these phenomena and predict the behavior of an object when changing the state parameters, and so the scope of these changes can be predetermined. One of the electromobility objects is a wheeled mobile platform. Wheeled mobile platforms are usually used for short-distance transport, and the vehicle is moved on a flat surface [1–3]. The movement of wheeled platforms is related to the interaction between road wheels and the ground. The effect of these interactions are deformations of contact zone wheel–ground and the frictional moment called the rolling friction torque [4]. Various methods of modeling wheeled mobile platforms' movement with determining track displacements on the basis of dynamic interactions have been presented in [1–3]. In each of these models, sliding friction forces were taken into account. However, the motion resistance resulting from deformations of the contact zone was omitted. The models of interaction between the wheel and the ground have been the subject of many studies focused on problems such as:

- energy dissipation during complex rotational motion of the spinning disc on a flat surface [5];
- application of the phenomenon of rolling friction in a design solution of the friction isolation system (a seismic isolator) [6];
- testing the effect of tire material properties on the tire-ice friction coefficient [7].

The original design solution of the wheeled mobile platform has been presented in the paper [3]. In order to develop the dynamic model of the platform, it is necessary to determine the dependence between force directly acting on the wheels F_y and rolling friction torque T. Therefore, developing a numerical model which will be used to determine such a relationship became the subject of this work. When selecting the modeling method in accordance with the guidelines contained in [4, 6], the mechanical properties of bodies in contact had to be taken into account. Taking into consideration the development of additive manufacturing techniques [8, 9], the Zortrax Z200 3D printer was used to produce the mobile platform's wheel. During 3D printing, the synthesis of plasticized filament takes place. As a result of this synthesis, the performed component

has a meso-structural structure. Cross-orientation of the structure generates free micro-spaces, the location of which is determined by the direction of movement of the 3D printer head. The experimental studies of the strength properties of such structures, which depend on the printer operating parameters, have been presented in the publication [10]. Taking into consideration the results of the work [11], it can be concluded that the printed platform's wheel will demonstrate orthotropic properties.

The effect of the macrotexture properties of the tire's top layer on the rolling friction torque has been demonstrated in work [12], but in the model of the contact zone, the local slip was omitted. Friction coefficients of the polymeric material that can be used during modeling the slip are included in the paper [13]. The extensive analytical model of rolling friction, taking into account the elliptical distribution of contact pressures, has been presented in the paper [14]. The problem of friction modeling was presented in the works [1–7, 14], but in any of the presented research methods the finite element method (FEM) for modeling has not been used. Taking into account the description of the classic model of rolling friction [4] and the orthotropic material properties of the platform's wheel [3], it was decided that the model of the wheel–flat surface system would be developed by using the finite element method. Therefore, the aim of this work is to develop a model for determining the rolling frictional torque associated with the rolling motion of the wheel on a flat surface, taking into consideration the susceptibility of the material structure and contact phenomena.

2. FEM model assumptions

Considering the conditions of modeling the motion of the mobile platform [3] and the classification of friction models presented in [15], it was assumed that a static friction model would be developed. The static friction model is shown schematically in Fig. 1.

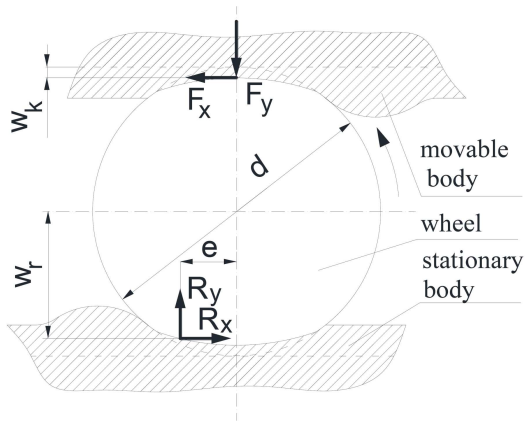

Fig. 1. The system of forces in the flexible model of rolling friction in contact zone roller–flat surface.

To map the conditions of cooperation between the platform's wheel with a diameter of $d = 200$ mm and the flat surface, it was assumed that the wheel would be subject to the resultant forces F_y. This force includes the range of loads resulting from the permissible weight, which will rest on the platform body. The translational and rotational movement will be caused by an action of resultant force F_x. This force in a real system results from the driving torque of an engine seated in the power train [16] and a sliding friction force, not indicated in Fig. 1 (the sliding friction force will be applied in the FEM model). In the present model, the forces F_y and F_x will be the active forces acting on the wheel. These forces will be introduced into the system through the moving body and contact conditions defined between the individual bodies of the model. Forces F_y and F_x cause deformations of bodies, especially deformations of the wheel w_k. Components R_x and R_y replace a resultant reaction, which is generated between the wheel and the stationary body. The position of the resultant reaction at the ground is determined by parameters e and w_r. The equation of static equilibrium condition for the assumed forces system has the following form

$$eF_y = F_x \left(\frac{d}{2} - w_k + w_r \right). \tag{1}$$

It follows from the above that the limit rolling friction torque will depend on the nature of the deformation in the contact zone, and the parameter identifying the deformation may be the distance e. Therefore, on the basis of the above assumptions, the rolling friction torque can be determined in the considered system based on the dependence

$$(ef(F_y)\,F)_y = T. \tag{2}$$

The parameters indicated above will be the input and output data of the FEM model. The values of R_x, R_y, e, and w_r will be determined based on the solution of a contact task in the contact zone of a cylinder–flat surface as a system of deformable bodies, which are loaded to external forces. In order to find the solution to (2), it is necessary for the FEM model to take into account the F_y force, which increases in steps, and the F_x force, which changes periodically. The sought unknown can be obtained by formulating the equations of equilibrium of 3D solid finite element nodes [17] subjected to loads and displacements in successive time steps Δt. Taking into consideration the natural behavior of the objects, it was found that they would experience large displacements and large rotations [17]. In order to solve this problem for all times $t + \Delta t$, an incremental Lagrange displacement analysis can be used. The analysis is based on the principle of virtual displacements described by [17]

$$\int_V {}^{(t+\Delta t)}\mathrm{d}V^{t+\Delta t}\tau_{ij^{(t+\Delta t)}}\,\delta e_{ij}^{(t+\Delta t)} = R^{(t+\Delta t)}, \tag{3}$$

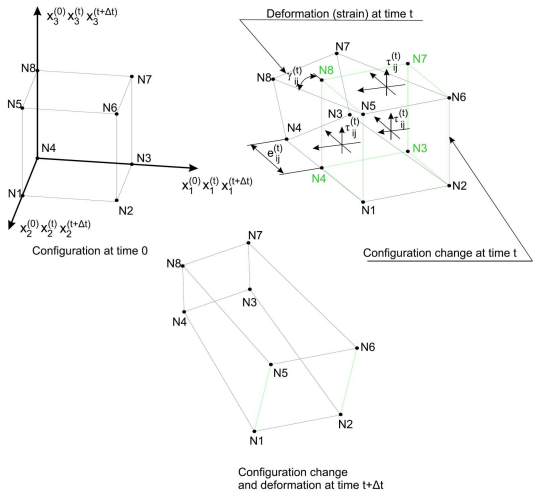

Fig. 2. Graphical interpretation of displacements and deformations of 3D solid finite elements.

where τ_{ij} is Cartesian components of the Cauchy stress tensor (internal force per unit area), e_{ij} — Cartesian components of the small strain tensor $i, j = 1, 2, 3$, and δ — variance operator. These parameters are expressed as

$$\delta e_{ij}^{(t+\Delta t)} \equiv \frac{1}{2}\left(\frac{\partial \delta u_i}{\partial x_j^{(t+\Delta t)}} + \frac{\partial \delta u_j}{\partial x_i^{(t+\Delta t)}}\right). \tag{4}$$

Infinitely small strain is related to the yet unknown configuration of the element. Hence, the variation of the deformation components is equivalent to the virtual strain during the virtual work of the body subjected to virtual displacements. External virtual work is given by

$$R^{(t+\Delta t)} = \int\limits_V^{(t+\Delta t)} \mathrm{d}V^{(t+\Delta t)}\, F_i^{B(t+\Delta t)} \delta u_i + \int\limits_S^{(t+\Delta t)} \mathrm{d}S^{(t+\Delta t)}\, F_i^{S(t+\Delta t)} \delta u_i, \tag{5}$$

where F_i^B is vector of volumetric forces, F_i^S — vector of surface forces, and δu_i — the i-th component of the virtual displacement vector.

The coordinates corresponding to the successive time steps with displacements in the single finite element, according to Fig. 2, are given by

$$x_i^{(t)} = x_i^{(0)} + u_i^{(t)}, \tag{6}$$

$$x_i^{(t+\Delta t)} = x_i^{(0)} + u_i^{(t+\Delta t)}. \tag{7}$$

For time t, the Piola–Kirchhoff stress tensor S_{ij} [17] is related to the initial (base) configuration of time $t = 0$. The designation used in the formulas below corresponds to (configuration; time step) or (time step)

$$S_{ij}^{(0;t)} = \frac{\rho^{(0)}}{\rho^{(t)}} \frac{\partial x_i^{(0)}}{\partial x_m^{(t)}} \tau_{mn}^{(t)} \frac{\partial x_j^{(0)}}{\partial x_n^{(t)}} \tag{8}$$

or after conversion

$$\tau_{mn}^{(t)} = \frac{\rho^{(t)}}{\rho^{(0)}} \frac{\partial x_m^{(t)}}{\partial x_i^{(0)}} S_{ij}^{(0;t)} \frac{\partial x_n^{(t)}}{\partial x_j^{(0)}}, \tag{9}$$

where $\frac{\partial x_m^{(t)}}{\partial x_i^{(0)}}$ is deformation gradient.

An important property of the Piola–Kirchhoff second type tensor is that its components are invariant during the rotation of the material body, i.e., the motion of the rigid body. The virtual work expressed by the above formula uses the Piola–Kirchhoff type stress tensor and the Green–Lagrange strain tensor as the basis for describing the incremental Lagrange equations used to describe non-linear structures of a continuous medium. Generally speaking, the body may experience large displacements and large deformations, the constitutive relationships are non-linear, and the relationship (3) cannot be solved directly. However, an approximate solution can be obtained for all the variables previously calculated with a known equilibrium (initial) configuration and linearization of the solutions to these equations. This solution can be improved by additional iterations. The formula called total Lagrangian (T.L.) has been used to develop directional equations for approximate solutions obtained by linearization. In this solution, all static and kinematic variables are related to the initial configuration over time $t = 0$. Thus, the reference may be made to a know configuration of stresses and strains. Therefore, the T.L. formula takes into account all kinematic non-linear effects resulting from large displacements and large rotations, but in the case of large deformations, the modeled displacements depend on the constitutive equations. Using an approximation based on constitutive law, i.e.,

$$S_{ij}^{(0)} = C_{ijrs}^{(0)}\, e_{rs}^{(0)}, \tag{10}$$

$$\delta \varepsilon_{ij}^{(0)} = \delta e_{ij}^{(0)}, \tag{11}$$

the following approximations of the equation of motion is obtained

$$\int\limits_V^{(0)} \mathrm{d}V^{(0)}\, C_{ijrs}^{(0)} e_{rs}^{(0)}\, \delta e_{ij}^{(0)} + \int\limits_V^{(0)} \mathrm{d}V^{(0)}\, S_{ij}^{(0;t)}\, \delta \left[\frac{1}{2} \frac{\partial u_k}{\partial x_i^{(0)}} \frac{\partial u_k}{\partial x_j^{(0)}}\right] = R^{(t+\Delta t)} - \int\limits_V^{(0)} \mathrm{d}V^{(0)}\, S_{ij}^{(0;t)}\, \delta e_{ij}^{(0)}. \tag{12}$$

The constitutive law based on the generalized Hooke's law, in which the component of material constants is written in the form of a C_{ijrs} tensor, can be included in the vector–matrix notation proposed by Voigt. According to Voigt's notation for the generalized Hooke's law, the tensor C_{ijrs} is reduced to the stiffness matrix C_{ij}. The components of the finite element stiffness matrix used to model objects with isotropic properties are as follows [17]

$$C_{ij} = \frac{E}{1+\nu}\begin{bmatrix} \frac{1-\nu}{1-2\nu} & \frac{\nu}{1-2\nu} & \frac{1-\nu}{1-2\nu} & 0 & 0 & 0 \\ & \frac{1-\nu}{1-2\nu} & \frac{1-\nu}{1-2\nu} & 0 & 0 & 0 \\ & & \frac{1-\nu}{1-2\nu} & 0 & 0 & 0 \\ & & & \frac{1}{2} & 0 & 0 \\ & \text{symmetric} & & & \frac{1}{2} & 0 \\ & & & & & \frac{1}{2} \end{bmatrix}. \tag{13}$$

where E is the Young's modulus and ν is the Poisson's ratio.

On the other hand, the components of the stiffness matrix of finite elements used to model objects with orthotropic properties are as follows

$$C_{ij} = \begin{bmatrix} \frac{1-\nu_{bc}\nu_{cb}}{E_b E_c \Delta} & \frac{\nu_{ba}+\nu_{bc}\nu_{ca}}{E_b E_c} & \frac{\nu_{ca}+\nu_{ba}\nu_{cb}}{E_b E_c \Delta} & 0 & 0 & 0 \\ & \frac{1-\nu_{ac}\nu_{ca}}{E_a E_c \Delta} & \frac{\nu_{ba}+\nu_{bc}\nu_{ca}}{E_b E_c \Delta} & 0 & 0 & 0 \\ & & \frac{1-\nu_{ab}\nu_{ba}}{E_a E_b \Delta} & 0 & 0 & 0 \\ & & & G_{bc} & 0 & 0 \\ & \text{symmetric} & & 0 & G_{ac} & 0 \\ & & & 0 & 0 & G_{ab} \end{bmatrix}. \tag{14}$$

where

$$\Delta = \frac{1-\nu_{ab}\nu_{ba}-\nu_{bc}\nu_{cb}-\nu_{ca}\nu_{ac}-2\nu_{ba}\nu_{cb}\nu_{ac}}{E_a E_b E_c}. \tag{15}$$

Due to the fact that the stiffness matrix is created as a result of the operation of the susceptibility matrix inversion, the constants of the orthotropic material state must realize the following relationships

$$E_i G_{ij} > 0, \tag{16}$$

$$|\nu_{ij}| < \sqrt{\frac{E_i}{E_j}}, \tag{17}$$

where $i, j = a, b, c$, and

$$\nu_{ba}\nu_{cb}\nu_{ac} < \frac{1}{2}\left(1-\nu_{ab}\nu_{ba}-\nu_{bc}\nu_{cb}-\nu_{ac}\nu_{ca}\right) < \frac{1}{2}\left(1-\nu_{ba}^2\left(\frac{E_a}{E_b}\right)-\nu_{cb}^2\left(\frac{E_b}{E_c}\right)-\nu_{ac}^2\left(\frac{E_c}{E_a}\right)\right). \tag{18}$$

3. Determination of the stiffness matrix parameters for a meso-structural body

The final stage of creating the FEM model is determining the parameters of a material model. The modeled wheel of the mobile platform is made of the material which is called acrylonitrile butadiene styrene (ABS).

In the works [18, 19], it was demonstrated that the printed components represent orthotropic properties. This means that the values of strain and stresses will depend not only on the directions and values of loads but also on the directions defining the main working plane of the printer. Therefore for modeled wheel, orthotropic axes (abc) have been introduced in accordance with the main plane of printing (ab). In the 3D printing process, successive layers are superimposed on the ab plane along the c axis (Fig. 3b). In order to determine parameters of the constitutive law for the 3D solid finite element (see (14)), such as directional: Young's modulus, Kirchhoff's modulus, and Poisson's ratio, a static tensile test, and a static torsion test were performed. The tests used 5-fold cylindrical samples with a diameter of 6 mm.

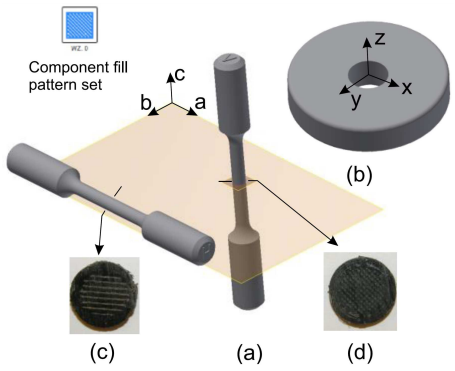

Fig. 3. Orientation of the main plane of 3D printing of samples (a), wheel of platform (b). Photos of cross-sections of samples made in accordance with horizontal (c) and vertical (d) orientation.

The samples were printed in two orientations (horizontal and vertical) relative to the main plane of the print ab, as shown in Fig. 3a. A arrangement of fibers in the cross-section of the samples for given a printout orientation is shown in Fig. 3c (horizontal orientation) and Fig. 3d (vertical orientation).

The average relationships stress–strain is σ–ε and torsion torque–torsion angle — M–Φ.

Based on the experimentally obtained relationship σ–ε, the directional Young's modulus E_a=E_b, Poisson's ratios $\nu_{ab} = \nu_{ba}$, and tensile strength R_{am}=R_{bm} were determined for samples made in a horizontal orientation. For samples made in

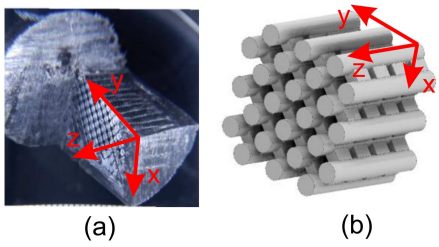

Fig. 4. Finite element mesh of model wheel–ground.

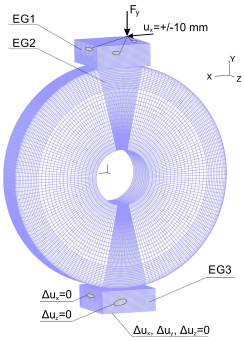

Fig. 5. Photo of permanent deformation (a) and idealized geometric form (b) of the considered meso-structure.

a vertical orientation the directional Young's modulus E_c, Poisson's ratio $\nu_{ca} = \nu_{cb}$, and tensile strength R_{cm} were determined. Whereas the relationship M–Φ allowed to determine shear modulus $G_{bc} = G_{ac}$ for samples made in a horizontal orientation and shear modulus G_{ab} for samples made in a vertical orientation. These values for Fig. 4 are included in Table I.

In order to visually identify the meso-structure, the sample was subjected to a shear load. The form of permanent deformation of the structure is shown in the photo (Fig. 5a). Whereas the idealized geometric model of the considered meso-structure is visualized in Fig. 5b. The identified structure allows to confirm that the printed wheel will demonstrate the transverse-orthotropic properties, which are described by the parameters given in Table I.

4. FEM model of the contact zone wheel–ground

Based on the assumptions presented above, using the ADINA system [20], the finite element mesh for the model shown in Fig. 1 was generated.

The meso-structure in the geometrical model of the wheel has been replaced by a uniform solid, which is subjected to discretization by using finite elements of the type 3D solid [17, 20]. The directivity of the identified structure was taken into account by considering the finite elements of the model as structures with orthotropic properties, which are

TABLE I

Parameters list of the stiffness matrix for all finite elements groups of the model (Fig. 4).

Finite element group	Parameters of the stiffness matrix defined in the model
EG1	according to (13)
	$E = 200000$ MPa,
	$\nu = 0.3$,
EG2	according to (14)
	$E_a = E_b = 1026$ MPa,
	$E_c = 1115$ MPa,
	$\nu_{ab} = \nu_{ba} = -0.54$,
	$\nu_{ca} = \nu_{cb} = -0.38$,
	$G_{ab} = 425$ MPa,
	$G_{bc} = G_{ac} = 405$ MPa,
	$R_{am} = R_{bm} = 26$ MPa,
	$R_{cm} = 20$ MPa,
EG3	according to (13)
	$E = 200000$ MPa
	$\nu = 0.3$

described by parameters given in Table I. The main plane of the print xy of the 3D printer (Fig. 3) was replaced in the FEM model (Fig. 4) with the xy plane. In this way, the orthotropic properties of the meso-structure of the wheel resulting from the specificity of the 3D printing process were mapped.

The finite elements of the model were grouped into three sets, which have been represented in Fig. 1 and Fig. 4. Set EG1 is the movable body, EG2 — wheel, and EG3 — stationary body. The stiffness matrix for the finite elements of the EG1 and EG3 groups was defined for isotropic bodies, i.e., according to (13), but in the case of the EG2 group, the stiffness matrix was defined according to (14). The numerical data introduced into the model are listed in Table I. External located nodes of the EG3 group have had taken their freedom of movement. An unknown value of the F_x force (Fig. 1) in the FEM model was replaced by the u_x displacement. Load F_y and displacement u_x are defined in a common node. Displacements of this node have been linked to the exterior nodes of EG1 group by using conditions of constraint type [20]. Node to node type contact conditions [17, 20] have been defined between exterior located nodes of the groups EG1–EG2 and EG2–EG3. This type of contact takes into account the sliding friction. In the FEM model, the value of the sliding friction coefficient $\mu = 0.2$ was introduced. The load was implemented through the F_y vector. Value of F_y force was proportionally increased for subsequent time steps. For the successively obtained equilibrium conditions, a displacement of $u = \pm 10$ mm amplitude was implemented.

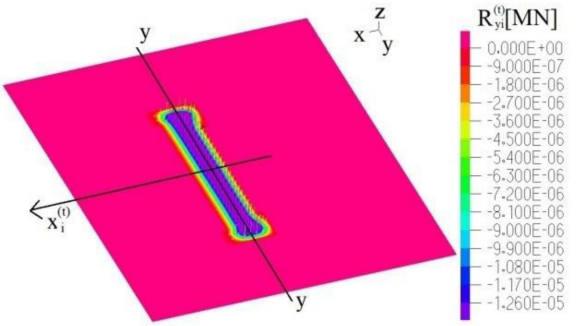

Fig. 6. Distribution of contact reactions in the contact zone wheel–stationary body.

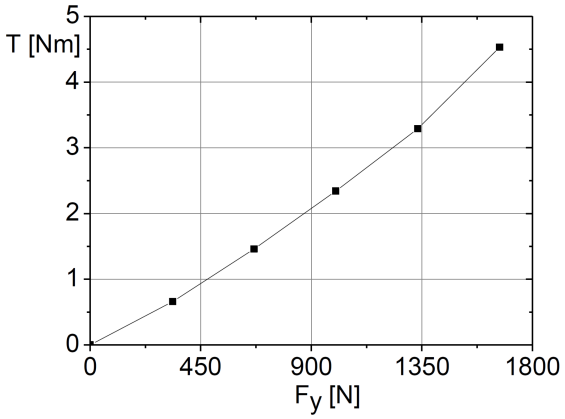

Fig. 7. Relationship of the rolling friction torque T on the force of wheel pressure F_y on the ground.

Static linear equilibrium equations for finite elements of the model considering constitutive laws, implemented into matrix form in the ADINA system, were solved using a sparse matrix solver. This solver is based on the Gaussian elimination method. The non-linear equations resulting from the need to solve the contact problem were solved iteratively based on the Full Newton method. The convergence of solutions between successive time steps (iterations) of calculations was determined by the defined value of tolerance for strain energy and contact force tolerance. The strain energy tolerance was ETOL = 0.001, and the contact force tolerance was RCTOL = 0.05. This means that the ratio of strain energy between two consecutive steps must be less than the ETOL value. For the contact force quotient, it is similar [20].

5. Calculation results

The solution to the task described above was the calculated reactions and displacements of nodes in the contact zone (Fig. 6).

The load entered into the model mapped the rotational and translational motion of the wheel on a flat surface, taking into account the susceptibility of contact zone. In order to determine the dependence between the frictional torque T and F_y force, it was necessary to determine the position e of the resultant reaction R_y (Fig. 1). This position can be identified on the basis of a distribution of the reaction components in a contact zone. For this purpose, it can be used as the method of determining the center of parallel forces. Knowing the values of the reaction components in the i-th nodes of the contact zone, $R_{yi}^{(t)}$, and the coordinates of these nodes in a deformed state, $x_i^{(t)}$, the value of $e^{(t)}$ for the subsequent time steps t can be determined according to the formula

$$e^{(t)} = \frac{\sum\limits_i R_{yi}^{(t)}\, x_i^{(t)}}{\sum\limits_i R_{yi}^{(t)}}. \tag{19}$$

(Note that designations of node coordinates are compatible with the description specified in Figs. 1 and 4). Considering the position $e^{(t)}$ determined for the subsequent time steps t, it was found that the value of this position changes monotonically with increasing F_y force. Based on (2), a relationship of the rolling friction torque with the pressure force acting on the platform's wheel was determined. The relationship is shown in Fig. 7.

The relationship obtained for simulated model conditions (see Fig. 7), can be approximated by a function

$$T = 6 \times 10^{-7}\, F_y^2 + 0.001\, F_y + 0.009. \tag{20}$$

(Note that the approximation does not apply to the calculation results for the time step $t = 0$). Coefficient of determination for the function approximation is $R^2 = 0.999$.

6. Conclusions

The presented method of determining the rolling friction torque can be used for a similar study of contact pair systems. The calculation results presented in the form of relationship (20) will depend on the diameter of the wheel and the data describing the material model of the contact pairs. In the studied object, the meso-structure has a structure similar to composites and demonstrates orthotropic properties. Therefore, using FEM, it can be modeled as a homogeneous body with orthotropic-oriented properties. The model can be used for static and fatigue strength tests in the range of limit states for contact and reduced stresses. While creating FEM models of the studying system, it must be taken into account that this system will be subject to large displacement, large rotation, and in the case of the tested meso-structure, small strain. A comprehensive model of kinematics and dynamics of the wheeled mobile platform [3], taking into account the relationship (20), will be the subject of future publication.

References

[1] R. Carelli, G. Forte, L. Canali, V. Mut, G. Araguas, E. Destefanis, *Mechatronics* **18**, 187 (2008).

[2] D. Pazderski, *J. Intell. Robot. Syst.* **85**, 553 (2017).

[3] A. Jaskot, B. Posiadała, S. Śpiewak, *Mech. Res. Commun.* **83**, 58 (2017).

[4] S. Sasaki, Y. Namba, T. Iwanari, Y. Kitano, arXiv:2111.06258v1, 2021.

[5] D. Ma, C. Liu, Z. Zhao, Hongjian Zhang, *Proc. R. Soc. A* **470**, 20140191 (2014).

[6] S. Li, B. Wei, C. Zuo, X. He, *Shock Vib.* **2019**, 7473031, (2019).

[7] H. Mousavi, C. Sandu, *J. Terramech.* **91**, 319 (2020).

[8] H. Brooks, S. Molony, *Mater. Design* **90**, 276 (2016).

[9] M.K. Thompson, G. Moroni, T. Vaneker, *CIRP Annals*, **65**, 737 (2016).

[10] G. Alaimo, S. Marconi, L. Costato, F. Auricchio, *Compos. B: Eng.* **113**, 371 (2017).

[11] M. Somireddy, A. Czekanski, *Mater. Design* **195**, 108953 (2020).

[12] M. Kane, E. Riahi, M.-T. Do, *Coatings* **11**, 538 (2021).

[13] I. Gunes, T. Uygunoğlu, A. Evcin, B. Ersoy, *Acta Phys. Pol. A* **132**, 599 (2017).

[14] F. Marques, P. Flores, J.C. Pimenta Claro, H.M. Lankarani, *Multibody Syst. Dyn.* **45**, 223 (2019).

[15] J. Awrejcewicz, G. Kudra, *Eur. J. Mech. A/Solids* **42**, 358 (2013).

[16] A. Jaskot, B. Posiadała, S. Śpiewak, in: *Proc. 13th Int. Scientific Conference, RESRB 2016, Lecture Notes in Mechanical Engineering*, Eds. E. Rusiński, D. Pietrusiak, Springer, 2017.

[17] K.J. Bathe, *Finite Element Procedures*, Prentice-Hall, Upper Saddle River (NJ) 1996.

[18] I.B. Ishak, D. Fleming, P. Larochelle, *Mech. Based Des. Struct. Mach.* **47**, 583 (2019).

[19] H. Zhang, L. Cai, M. Golub, Y. Zhang, X. Yang, K. Schlarman, J. Zhang, *J. Mater. Eng. Perform.* **27**, 57 (2018).

[20] *ADINA, Theory and Modeling Guide*, Vol. 1, ADINA R&D, Inc. Watertown, 2012.